



# Evaluation of microstructure and toughness of SAW steel weld metals with optimum Al/O ratio

Kangmyung Seo<sup>1</sup> · Yongjoon Kang<sup>2</sup> · Hee Jin Kim<sup>3</sup> · Byungchul Kim<sup>4,5</sup> · Namhyun Kang<sup>5</sup>

Received: 11 October 2023 / Accepted: 27 February 2024 / Published online: 5 March 2024  
© International Institute of Welding 2024

## Abstract

A study was made to understand the possible effect of the Al/O ratio on the Charpy V-notch impact properties of submerged arc weld metals within the optimum range of Al/O ratio previously reported to be 0.45–0.75. To vary the Al/O ratio of weld metals in such a narrow range, two base plates different in aluminum content were selected, and a bead-in-groove weld was made on each plate using the same welding condition. From the chemical compositions obtained, the Al/O ratio of each plate was determined to be 0.47 and 0.75. Charpy impact tests showed that the ductile–brittle transition temperature (DBTT) of a low Al/O ratio was about 25 °C lower than that of a high Al/O ratio. The improvement in toughness is concluded to be attributable to the microstructural refinement that can be quantified by two different parameters: AF content increased from 70 to 79% and grain size decreased from 8 to 6 μm. These results also indicated that even a slight variation in aluminum content of base plates could cause a marked variation in weld microstructure and toughness. In addition, the inclusions in the weld of low Al/O ratio were confirmed to be covered by the TiO layer, but no manganese-depleted zone (MDZ) was observed.

**Keywords** Weld microstructure · Acicular ferrite · Weld toughness · Grain size · Manganese-depleted zone (MDZ)

## 1 Introduction

This work concerns the metallurgical relationship among weld metal chemistry, microstructure, and properties of C-Mn steel welds, a field in which significant advances have been achieved for the last 50 years. It is now well established that a high proportion of acicular ferrite (AF)

generally results in improved weld metal toughness, and the AF content is closely related to many metallurgical factors, one of them being the characteristics of non-metallic inclusions formed in weld deposits [1–4]. As demonstrated in the previous studies [5–8], inclusions in many welds act as nucleation sites for the AF plates, but in some welds, they do not tend to nucleate ferrites. Accordingly, the compositional factors related to the nucleation potency of inclusions have been the subject of numerous investigations [2, 9, 10].

For the compositional factors, titanium would be unique for AF formation from the weld microstructure point of view [11–17]. It is because as small as 10 ppm level dramatically changes the weld microstructure from the one dominant with the ferrite with second phase (FS) to the one with AF [17]. Such a change in weld microstructure was explained by the distinct differences in inclusion characteristics between titanium-free and titanium-added weld metals. For example, the inclusions formed in the titanium-containing welds were often found to be covered with a titanium-rich phase that has long been believed to promote ferrite nucleation. Accordingly, titanium addition has become popular in designing welding consumables for improved toughness.

From the weld metal toughness point of view, controlling aluminum and oxygen contents appears to be as important

Recommended for publication by Commission IX - Behaviour of Metals Subjected to Welding

✉ Hee Jin Kim  
kimheejin0827@gmail.com

- <sup>1</sup> Hyundai Steel Co., Bukbusaneop-ro, Songak-eup, Dangjin-si 1480, Chungcheongnam-do, Korea
- <sup>2</sup> Korea Institute of Materials Science, 797, Changwon-Daero, Seongsan-Gu, Changwon-Si 51508, Gyeongsangnam-do, Korea
- <sup>3</sup> R&D Center, KISWEL, 704 Gongdan-Ro, Seongsan-Gu, Changwon-Si 51544, Gyeongsangnam-do, Korea
- <sup>4</sup> HD Korea Shipbuilding & Offshore Engineering, 477, Bundangsuseo-ro, Bundang-gu, Seongnam-si, Gyeonggi-do, Korea
- <sup>5</sup> School of Material Science, Pusan National University 2, Busandaehak-ro 63, Geumjeong-gu, Busan 46241, Korea

as titanium addition because the weld microstructure and toughness have been reported to be significantly affected by the wt.% aluminum-to-wt.% oxygen ratio (Al/O ratio) of the welds [18–20]. For example, as shown in Fig. 1, Horii [18] reported that the 50% fracture appearance transition temperature (FATT) of low alloy weld metals strongly depends on the Al/O ratio of weld metal. Despite some scattering, this result demonstrates that the weld toughness improves the most when the Al/O ratio is between 0.45 and 0.75, suggesting the existence of an optimum range in the Al/O ratio for the weld toughness [10, 19]. On the other hand, Terashima and Hart [20] reported the improvement of weld toughness being obtained at  $(\text{wt.\% Al})/(\text{wt.\% O})^2$  ratio of about 28. The two optimum conditions can be satisfied simultaneously when the oxygen content is controlled to be 0.022% at 0.013% aluminum. Following Horri's results of optimum Al/O ratio being 0.45–0.75, many researchers, mainly in Japan, have investigated the inclusion characteristics and found that those inclusions formed in the welds of optimum Al/O ratio were covered with TiO layer, a phase having low lattice misfit with ferrite and thus believed to promote ferrite nucleation [5, 21, 22].

Recently, Fujiyama and Shigesato [23] have measured the ductile–brittle transition temperature (DBTT) of the submerged arc welds having different Al/O ratios of 0.48 and 1.00 and showed that the weld with low Al/O ratio exhibited much lower DBTT than that of high ratio. This result confirms that weld toughness properties are a function of the Al/O ratio and thus can be improved by controlling the Al/O ratio to be in the optimum range. However, they did not pay an attention on the possible variation of impact properties

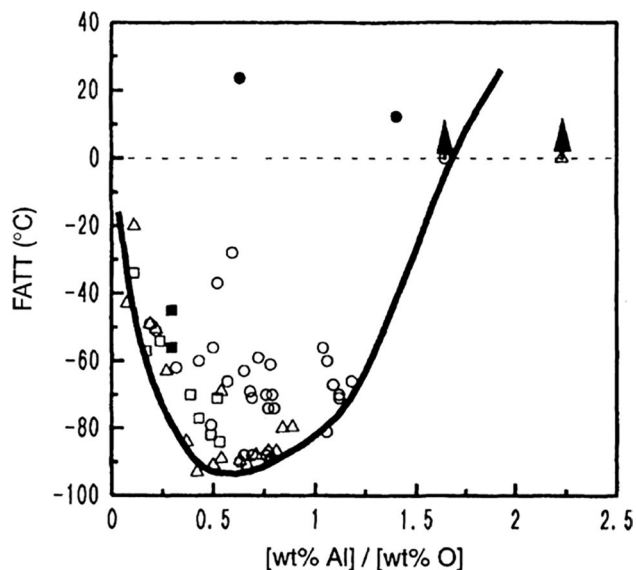


**Fig. 1** Effect of Al/O ratio on 50% FATT of low alloy weld metals [18]

within the optimum range of 0.45–0.75. Thus, the effect of Al/O ratio is not clear yet within this optimum range. For the inclusion characteristics, they could verify the formation of TiO layer on the inclusion surface, as reported by many investigators [5, 21, 22, 24]. Interestingly, however, they observed the manganese-depleted zone (MDZ) developed in the steel matrix adjacent to the TiO/steel interface, reducing the manganese concentration by about 1 at.%, the greatest at the interface. Following this observation, they claimed that, in addition to the low misfit mechanism, the MDZ mechanism is proposed to be operating with the TiO layer. However, their result of MDZ formation is far different from what the present authors observed in the electro-gas welds in which no MDZ was found even though the inclusions were well covered with a TiO layer [25]. The absence of MDZ formation associated with the TiO layer was also reported by other researchers [24, 26].

Historically, MDZ issues in weld metals have followed the early studies made with the steel plates that could be heat-treated for a long time at high temperatures [27–29]. As their results clearly showed that AF nucleates in heat-treated steels associating with the increased chemical driving force by the MDZ formed around the  $\text{Ti}_2\text{O}_3$  inclusions, welding researchers have looked into the inclusions to see if MDZ could be formed even in the rapid-cooling weld thermal conditions. Like in steel plates, the weld inclusions composed of  $\text{Ti}_2\text{O}_3$  were found to be active for MDZ formation [30, 31]. Later, many researchers found that the inclusions containing (Mn,Ti) oxide also formed MDZ [32–36]. However, as mentioned above, it is arguable whether or not MDZ forms when the inclusion is coated by the TiO layer.

In steel welds, base metal dilution is unavoidable and its extent is normally as high as 60% in SAW process especially in the case of single run or both-side one-run procedures. For these welds, therefore, the aluminum content of SAW weld is strongly influenced by that of base metals that normally varies from 0.2 to 0.5% so that the Al/O ratio of welds varies even with the same welding consumables and conditions. Therefore, this work aimed to demonstrate the possible variation of toughness properties of submerged arc welds made with base metals different in aluminum content, and by the careful selection of based metals, it was also intended to fall the Al/O ratio within a range of 0.45–0.75, which has previously been reported as an optimum range. Two submerged arc welds different in Al/O ratio were prepared to facilitate this goal: one close to the lower limit and the other to the upper limit. In addition, it was intended to characterize the inclusions and to make sure the presence or absence of MDZ when the inclusions are covered with TiO layers.

## 2 Experimental procedure

The submerged arc welds investigated in this study were prepared by bead-in-groove welding technique using two base metals, both steels being classified as the EH36 grade in ship classification societies [37]. Referring to the mill test certificates, the yield strength of both steels is over 440 MPa and the tensile strength is over 510 MPa, and the Charpy impact toughness is well over 300 J at  $-40\text{ }^{\circ}\text{C}$ . To vary the Al/O ratio of the welds, two base plates were carefully selected to be similar in chemistry except for aluminum. Table 1 shows the chemical composition of the plates used in the present study. The aluminum content of the low-aluminum plate designated BL is 0.030 wt.% while that of high-aluminum plate, BH, is 0.043 wt.%. Other major alloying elements, like carbon, silicon, and manganese, are nearly identical in their contents.

For the bead-in-groove welding, a  $60^{\circ}$  V-groove was machined on the 22-mm-thick  $1000\times 200$ -mm steel plates to a depth of 6 mm. The groove was completely filled by a single pass using a single-wire submerged arc welding (SAW) process with a heat input of 3.57 kJ/mm. The welding parameters were 700 A–34 V–400 mm/min, and the contact tip to work distance was 30 mm. The flux and wire combination used were the one classified as AWS F7A8-EH14, and the basicity of the flux is 2.5. Figure 2a shows the macrostructure taken from the transverse cross section of the welds made. Chemical analysis was carried out using an optical emission spectrometer (OES) except oxygen and nitrogen being determined by the vacuum fusion method

using Leco analyzer, and the results are presented in Table 1 along with the base metal chemistries.

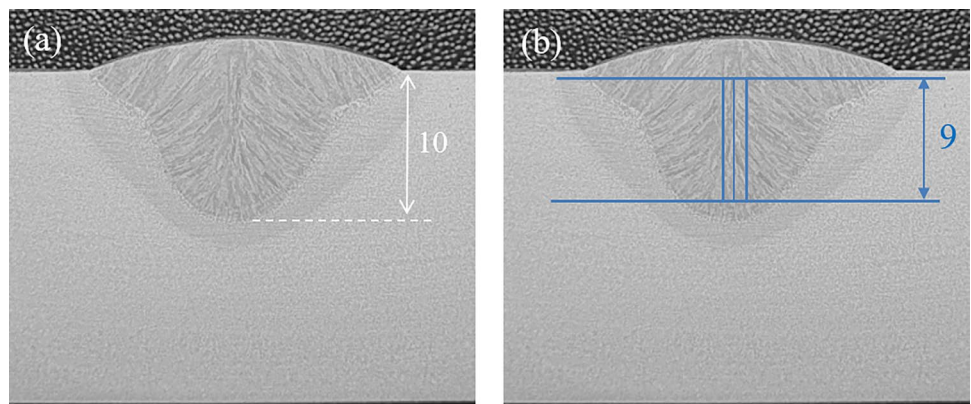
The toughness of each weld was assessed by the Charpy V-notch test with the sub-thickness specimens taken as shown in Fig. 2b. The specimens were all oriented transverse to the welding direction and notched on the weld center. Due to the limited depth of the welds made, the thickness of Charpy specimens was determined to be 9 mm instead of the standard, 10 mm. Sufficient tests were conducted at various temperatures to construct the full ductile–brittle transition curves for each weld [38].

Quantitative metallography was also done on the transverse cross sections etched with 2% Nital solution to measure the area fraction of three major constituents: grain boundary ferrite (GBF), FS, and AF. The proportion of each constituent was determined by the point counting analysis using 10 optical micrographs taken at a magnification of  $\times 200$ . The same specimens were used for the scanning electron microscopy (SEM)/electron backscattered diffraction (EBSD) analysis to measure the grain size after re-polishing with colloidal silica in a vibratory polisher. EBSD images were taken at a magnification of  $\times 500$  using a step size of  $0.5\text{ }\mu\text{m}$ . The grain size was determined by the equivalent circle diameter of grains surrounded by boundaries with a tolerance angle of  $15^{\circ}$ , or higher. Inclusion characterization was performed by analytical transmission electron microscopy (ATEM) equipped with energy-dispersive spectroscopy (EDS) operating at 200 kV. Selected area diffraction (SAD) analysis was also performed to identify the inclusion phases and their orientation relationship with AF

**Table 1** Chemical composition of base plates used and bead-in-groove welds made, wt.%

ID		C	Si	Mn	Al	Ti	O	N	Fe	Al/O
Base plate	BL	0.08	0.31	1.52	0.030	0.017	-	-	Remainder	-
	BH	0.07	0.33	1.53	0.043	0.011	-	-	Remainder	-
Weld metal	WL	0.08	0.37	1.53	0.017	0.022	0.036	0.003	Remainder	0.47
	WH	0.08	0.43	1.58	0.021	0.024	0.029	0.003	Remainder	0.72

**Fig. 2** Transverse macro specimen: **a** macrostructure and **b** notch location of Charpy specimen



matrix. Thin foil specimens for ATEM study were prepared by focused ion beam method.

### 3 Result

#### 3.1 Chemical composition of weld metals

Both base plates were selected from the ship-grade high-strength steels classified as AH36. Their compositions shown in Table 1 indicate that the ship-grade steels can have a wide variation in aluminum content which can affect its content in the weld deposits via base metal dilution. From the macrostructure shown in Fig. 2, the dilution ratio was estimated to be about 65%. Associating with such a high dilution ratio, the aluminum content of the weld (WH) made on a high-aluminum plate (BH) turned out to be 0.021 wt.% while that of the weld (WL) made on a low-aluminum plate (BL) was determined to be 0.017 wt.%. As the aluminum is a strong deoxidizer, the difference in aluminum content appears to affect the oxygen content of the weld as well; the higher the aluminum content, the lower the oxygen content. As a result, the Al/O ratio of WH reaches 0.72, which is

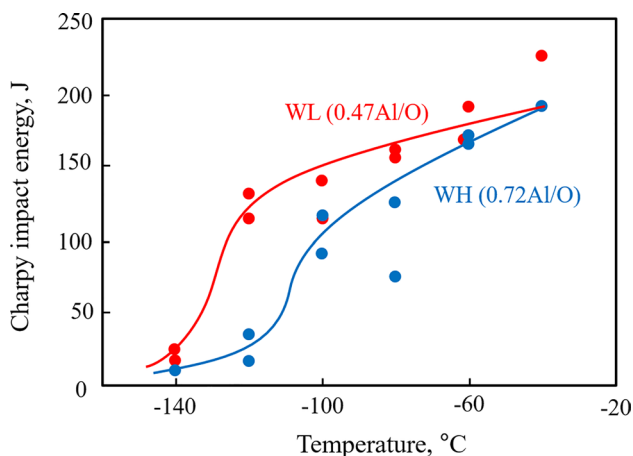
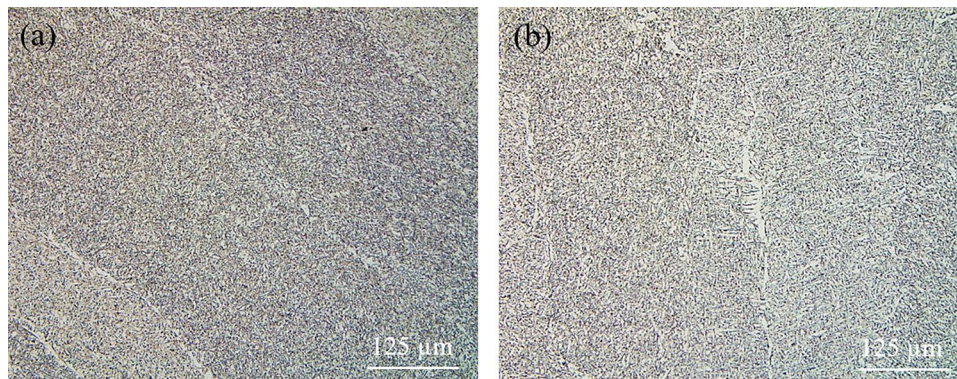


Fig. 3 DBTT curves constructed with 9-mm-thick Charpy specimens

Fig. 4 Optical micrographs of a WL and b WH weld metal



very close to the upper limit of the optimum range, while that of WL is 0.47, which is to the lower limit. Apart from aluminum and oxygen contents, other elements including titanium are similar in their contents as expected. Therefore, these two bead-in-groove welds were thought to be the ideal combination for the purpose of present study.

#### 3.2 Charpy impact toughness

Figure 3 shows the ductile–brittle transition curves constructed for WL and WH weld. From this result, it becomes clear that their transition curves are shifted to lower temperature side by changing the Al/O ratio from 0.72 to 0.47, demonstrating that even in the optimum range, the Al/O ratio notably influences the weld toughness. From the DBTT determined at impact energy of 100 J, the average value between the upper and lower shelf energies, it can be seen that the change in Al/O ratio from upper limit to lower limit suppresses DBTT from  $-100$  to  $-125$  °C, resulting in the toughness improvement as much as 25 °C suppression in DBTT. Following this result, it can be suggested for the present alloy system that the optimum range of Al/O ratio can be narrowed down close to its lower limit.

#### 3.3 Weld microstructure

Figure 4 shows the optical micrographs taken from WL and WH weld metals. They are composed mainly of AF with a small amount of GBF and FS. At a glance, WH weld appears to be higher in FS content than WL. This feature becomes clear in Table 2 that shows the proportion of each constituent determined by the point counting analysis. These results exhibit a pronounced difference between WL and WH especially in AF and FS contents. Correlating with the Al/O ratio, one can conclude that the decrease in Al/O ratio from 0.72 to 0.47 increases AF content from 70 to 79% with the corresponding decrease in FS content but has little effect on the content of GBF, which forms earlier than the other two constituents.

**Table 2** Result of quantitative analysis of weld microstructure

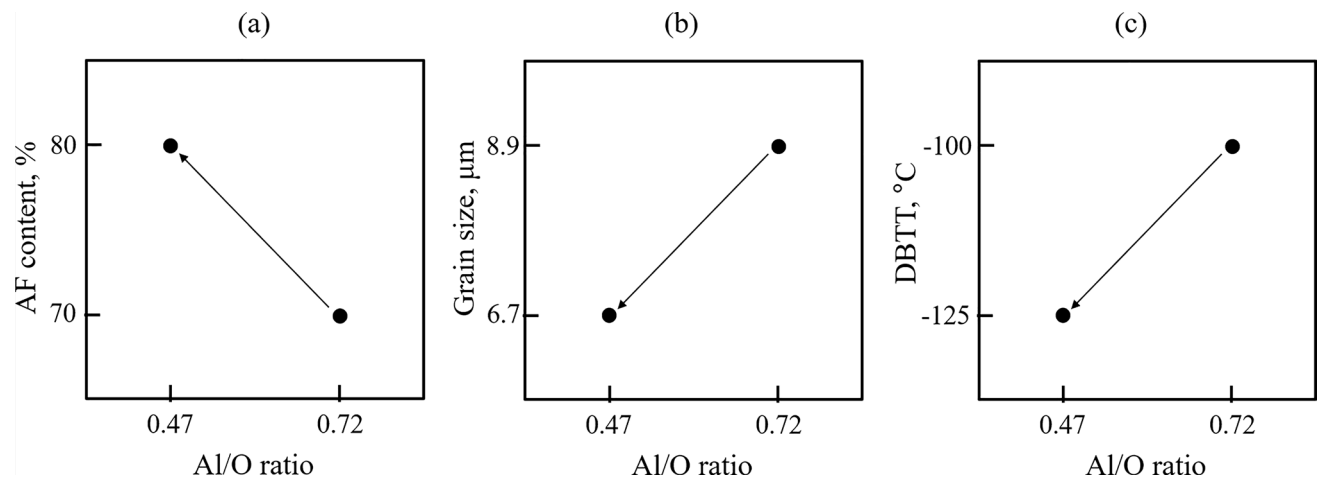
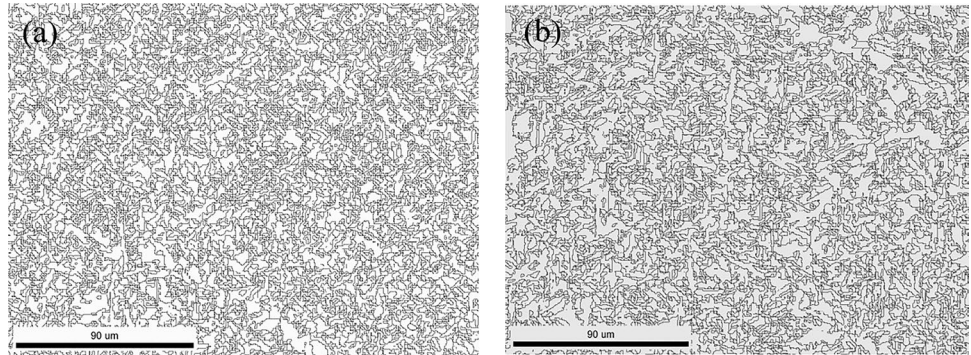
Weld ID		WL	WH
Optical/point counting	AF, %	78.8	69.8
	FS, %	11.8	18.2
	GBF, %	10.2	12.0
SEM/EBSD	Grain size, $\mu\text{m}$	6.08 ( $\pm 0.22$ )	8.48 ( $\pm 0.89$ )

Figure 5 shows the EBSD images depicting the grain boundaries determined with a tolerance angle of 15° or greater. The average grain size of five measurements for each weld is presented in Table 2 with the result of microstructural analysis. From this table, it can be seen that the grain size decreases from 8.5 to 6.1  $\mu\text{m}$  with the change in Al/O ratio from 0.72 to 0.47. This result suggests a relationship between grain size and AF content in that the grain size decreases with increasing AF content. This relationship is no wonder because AF grain structure is much finer than those of FS or GBF [39]. Therefore, it would be

possible to quantify the fineness of weld microstructure in terms of the average grain size of weld microstructure instead of AF content. The AF content is usually obtained from the microstructures taken by an optical microscope and has long been used in welding metallurgy to evaluate the weld metal microstructure quantitatively. In contrast, the grain size measured by SEM/EBSD technique was recently introduced and has little database in the literature. It is worth noting that grain size measured by EBSD represents the overall weld microstructure so it can reflect the fineness of all constituents including AF [40].

Figure 6 illustrates the effect of the Al/O ratio on the microstructural parameters of AF content and grain size, and on DBTT. From Fig. 6a, c, the lower DBTT of WL (0.47 Al/O) is explained in terms of the AF content increased, and this is a traditional interpretation popular in the welding metallurgy. According to Fig. 6b, c, however, the same feature can be explained in terms of the grain size decreased with decreasing Al/O ratio, and this is a way of interpretation normally employed in the field of steel metallurgy.

**Fig. 5** Typical EBSD grain structure of **a** WL and **b** WH weld metal



**Fig. 6** Effect of Al/O ratio on **a** AF content, **b** EBSD grain size, and **c** DBTT

### 3.4 MDZ formation

Prior to TEM specimen preparation, many inclusions of WL weld were examined in SEM/EDS and confirmed to have titanium-rich layers on the inclusion surface. This examination also showed that all the inclusions were essentially oxides with MnS or (Mn, Cu)S islands formed on the inclusion surfaces to a small extent. For three inclusions of over 1  $\mu\text{m}$  in size, TEM specimens were prepared to identify the crystal structure of titanium-rich layer and to investigate the presence or absence of MDZ adjacent to the inclusion surface.

A typical example of ATEM/EDS elemental mapping is shown in Fig. 7. Like this inclusion, all inclusions investigated were entirely covered with thin titanium-rich layer phase determined to be titanium oxide containing a small amount of nitrogen. This type of titanium-rich layer was also reported to be formed in the titanium-added steel material [41]. These layers were further analyzed through SAD and were determined to be TiO having the Baker-Nutting (B-N) orientation relationship with ferrite matrix. Figure 8 shows one of the SAD results showing the B-N relationship. The results shown in Figs. 7 and 8 are the same as the work reported by Fujiyama and Shigesato [23].

One of the major concerns in this study is identifying the MDZ formation because its formation was not in agreement among the previous investigators [23, 25, 26]. To alleviate the statistical issue, the present study examined all three inclusions that were well covered with TiO layer. For each inclusion, EDS scan analysis was conducted across the TiO layer at more than five different locations; however, no indication of MDZ formation was found. Figure 9 shows one of the typical results showing the manganese profile scanned across the TiO layer from the steel matrix, and demonstrating the absence of MDZ formation. This result is in total conflict with the previous findings of Fujiyama and Shigesato [23] even though, as mentioned, there is not much difference in chemistry including Al/O ratio.

## 4 Discussion

### 4.1 Effect of Al/O ratio

The aim of this paper is to investigate the effect of Al/O ratio on the weld metal toughness in the range of 0.45–0.75. The results show that even in such a narrow range, Al/O ratio has a profound effect on weld toughness associating

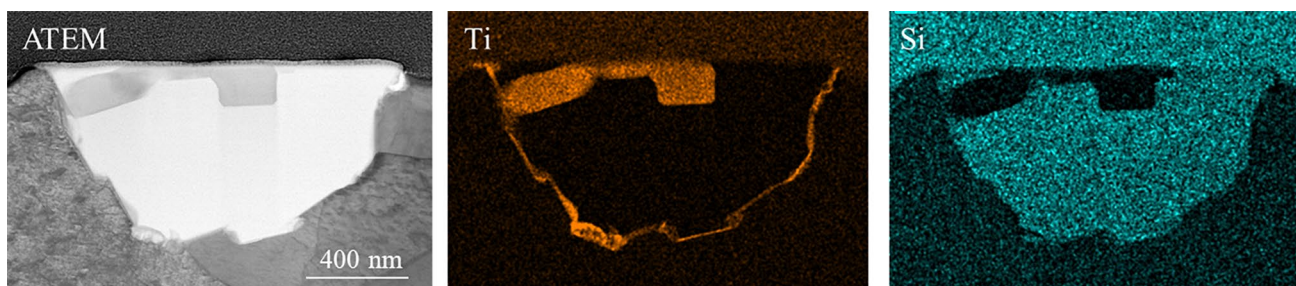


Fig. 7 Result of EDS mapping for titanium (Ti) and silicon (Si)

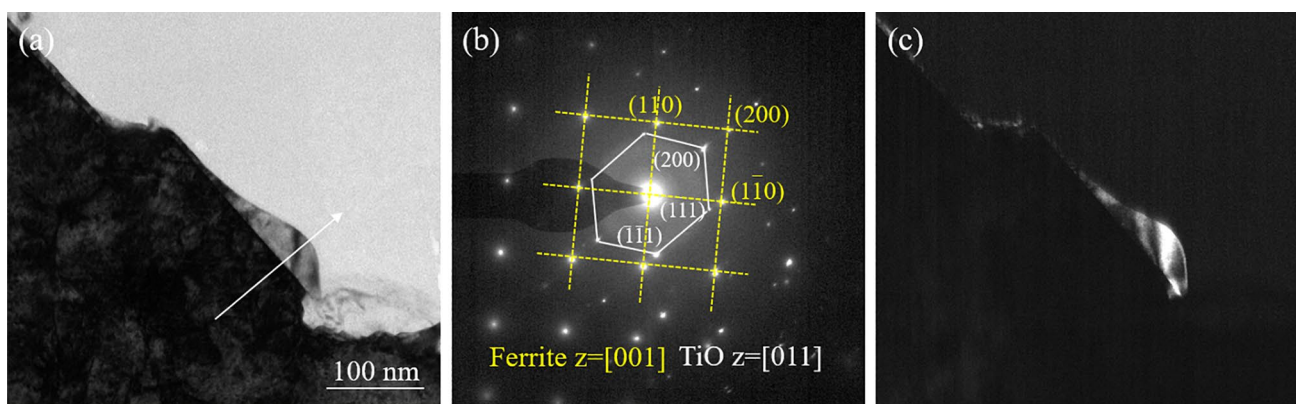
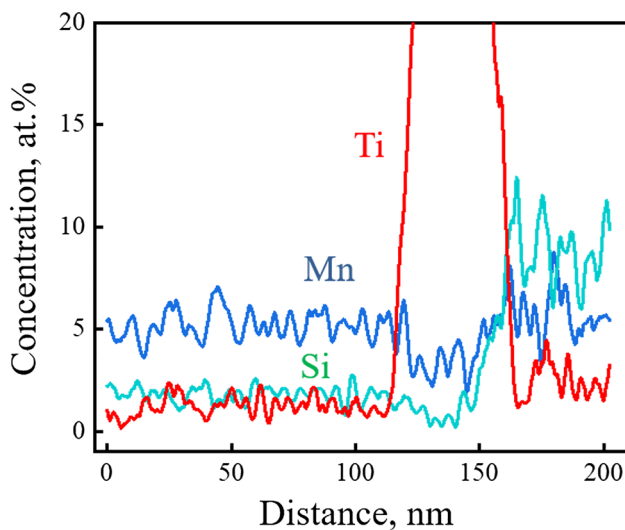


Fig. 8 Result of SAD analysis of TiO layer: **a** bright field image, **b** SAD pattern taken at the arrow-marked region, and **c** dark-field image taken from  $(11\bar{1})$



**Fig. 9** Result of EDS line scanning across the TiO layer following the arrow in Fig. 8a

with the change in weld microstructure. Based on the DBTT results shown in Fig. 3, it can be proposed to squeeze the optimum range by lowering the upper limit to some extent. To establish a new and narrower optimum range, extensive studies are certainly needed using a series of welds made with careful control in their composition.

Given that the aluminum content of steel plates varies widely from 0.02 to 0.05 wt.%, the weld toughness can be deteriorated to a great extent when the base metal dilution is great, which is shown in some of the welds, a typical example being a weld made with square-butt joint. In the case of multi-pass welds made with X-groove joints, the root pass would be the highest in base metal dilution compared to the subsequent passes. When the base metal is high in aluminum, such a high dilution makes the root pass high in Al/O ratio and thus results in low impact properties. Therefore, it is advised to consider the Al/O effect when studying the low toughness properties of the root area compared to the surface area.

## 4.2 MDZ formation

Another purpose of this study is to verify the MDZ formation recently reported by Fujiyama and Shigesato [23] in contrary to others [25, 26]. For the mechanism for MDZ formation, they conceived of two possibilities. The first is that on cooling, TiO phase can absorb manganese from the matrix, resulting in manganese depletion on the matrix side. This mechanism has been inferred from the MDZ formation numerously observed with  $Ti_2O_3$  inclusions [30, 31, 42, 43] and called the “cation vacancy effect” [42]. The other is the precipitation of Ti-Mn oxide at the austenite/inclusion interface, resulting in manganese depletion near the inclusion

surface and manganese enrichment in the TiO layer. As the manganese concentration in the TiO layer was shown to be higher than the ferrite matrix, they strongly suggested the manganese diffusion into the TiO layers. However, in this study, the manganese concentration in TiO layers was always lower than that of the steel matrix, as shown in Fig. 9. This fact indicates that there is no appreciable diffusion of manganese from the matrix into the TiO layer. As a result, no MDZ can take place in the present weld as demonstrated in Fig. 9.

Because of the little difference in chemistry between these two welds, it is not easy to discuss this discrepancy in MDZ formation; however, it may have something to do with the heat input employed. The heat input of the present weld is 3.6 kJ/mm, much lower than that of the weld used by Fujiyama and Shigesato [23]. Even if MDZ can be formed by the cation vacancy effect after solidification, the faster cooling rate resulted from a lower heat input limits the manganese diffusion to form MDZ. Considering the possible effect of cooling rate, the MDZ formation with TiO layer needs to be verified further by experiment using a series of submerged arc welds similar in composition but different in heat input.

## 4.3 EBSD grain size

Traditionally, based on the well-established relation between AF content and weld toughness, the weld microstructure has been often quantified into three major constituents such as GBF, FS, and AF, following the IIW guideline proposed by Pargeter and Dolby [44]. Among these three constituents, the primary concern would be the AF content, as it is a dominant factor controlling the weld toughness. In general, the area fraction of AF constituent can be determined by point counting method, the principles described by Davey and Widgery [45]. In the present work, the total number of counts was as high as 2000 per sample; thus, as one might suspect from this number, the point counting procedure is undoubtedly time-consuming and exhausting.

In the high-toughness weld metals, the weld microstructure contains a high proportion of AF, of which plates nucleate from the non-metallic inclusions. This phase forms below approximately 600 °C following the formation of GBF and Widmanstätten ferrite, a type of ferrite classified into FS in the scheme of IIW guideline [45]. During cooling below 500 °C, the remaining austenite between the AF laths transforms to bainite or microphases that are often called martensite-austenite (MA) constituents, indicating that these phases increase in their amount as the AF content increases. When etched in the Nital solution, considerable confusion surrounds identifying these phases from AF because these are finely distributed between the laths of AF. Therefore, another limitation of the point counting method seems to be an increased human error in analyzing the microstructure high in bainite or MA phases.

More importantly, throughout the optical observation performed for point counting procedure, the grain size character of weld microstructure is out of scope mainly because the AF grains are not clearly defined in the optical micrographs and highly irregular in shape. This feature becomes more severe in the high-toughness weld metals like the present welds. Considering the well-established relationship between grain size and DBTT, the AF grain size is certainly of more value than its proportion in the case of AF-dominant weld metals [40]. In other words, AF content alone is insufficient to characterize the weld metal microstructures of high-toughness welds due to the absence of grain size information. In fact, there seems to be no etching technique available at the moment that allows to reveal the grain structure of AF effective for blunting the brittle crack propagation.

For the morphological aspect, the aspect ratio of AF has been reported to be changed with weld chemistry [46]. However, whether the AF grain size changes by controlling weld chemistry or inclusion characteristics is not well studied. When the methodology to refine the AF microstructure is understood, further weld toughness could be improved for the welds predominant with AF, like the welds studied in this investigation. In this context, the EBSD technique is essential for better understanding weld microstructures in terms of grain size; EBSD grain size can be defined as a function of misorientation angle between adjacent two grains. In the practical aspects, EBSD method enables to save time in analyzing the weld microstructure compared to the point counting method and generates reliable data by eliminating human errors most likely elevated in high-toughness weld metals to some extent.

## 5 Conclusion

The possible effect of the Al/O ratio on weld toughness and microstructure was investigated using two bead-in-groove SAW weld metals, of which Al/O ratios are within the optimum range but close to lower and upper limits. From this study, the following conclusions can be drawn.

1. The DBTT obtained at the Al/O ratio of 0.47 was appreciably lower than that of 0.72 by 25 °C, suggesting a significant effect of the Al/O ratio on weld toughness even in the optimum range. This result indicates that even a small variation of aluminum content in base plates could cause a marked difference in weld toughness.
2. With decreasing the Al/O ratio, the AF content increased from 70 to 79% resulting in the grain size decrease from 8.5 to 6.1 μm. Hence, the toughness improvement obtained with the decrease in Al/O ratio is concluded to be attributed to the microstructural refinement which can be quantified in terms of AF content or the grain size.

The latter method was recommended considering the experimental errors likely less in the EBSD technique than the point counting method.

3. All inclusions were fully covered with thin TiO layers containing a small amount of nitrogen, and this layer had a B-N orientation relationship with ferrites nucleated from the inclusion, indicating that a mechanism of low lattice misfit is operating in these welds.
4. This study confirmed the absence of MDZ formation for the weld of 0.47 Al/O ratio. This result conflicts with the previous report even though the weld chemistry is similar. Therefore, MDZ formation associated with the TiO layer remains to be re-confirmed in weld metals similar in composition.

**Funding** This work was supported by the Korea Institute of Energy Technology Evaluation and Planning (KETEP) grant funded by the Korea government (MOTIE) (20206510100030, Development of Repair Technology for Class 2, 3 Large Bore Piping in Operating Nuclear Power Plant).

## Declarations

**Conflict of interest** The authors declare no competing interests.

## References

1. Abson DJ, Pargeter RJ (1986) Factors influencing as-deposited strength, microstructure, and toughness of manual metal arc welds suitable for C-Mn steel fabrication. *Int Met Review* 31(4):141–194
2. Sarma DS, Karasev AV, Jönsson PG (2009) On the role of non-metallic inclusions in the nucleation of acicular ferrite in steels. *ISIJ Int* 49(7):1063–1074. <https://doi.org/10.2355/isijinternational.49.1063>
3. Loder D, Michelis SK, Bernhard C (2017) Acicular ferrite formation and its influencing factors—a review. *J Mater Sci Res* 6(1):24–43. <https://doi.org/10.5539/jmsr.v6n1p24>
4. Xuan C, Mu W (2022) New insights of heterogeneous nucleation and anisotropic growth of acicular ferrite on non-metallic inclusion. *Mater Des* 221(9):110892. <https://doi.org/10.1016/j.matdes.2022.110892>
5. Yamada T, Terasaki H, Komizo Y (2009) Relation between inclusion surface and acicular ferrite in low carbon low alloy steel weld. *ISIJ Int* 49(7):1059–1062. <https://doi.org/10.2355/isijinternational.49.1059>
6. Seo JS, Lee C, Kin HJ (2013) Influence of oxygen content on microstructure and inclusion characteristics of bainitic weld metals. *ISIJ Int* 53(2):279–285. <https://doi.org/10.2355/isijinternational.53.279>
7. Horii Y, Ichikawa K, Ohkita S, Ohkita S, Funaki S, Yurioka N (1995) Chemical composition and crystal structure of oxide inclusions promoting acicular ferrite transformation in low alloy submerged arc weld metal. *Quarterly J Jap Weld Soc* 13(4):500–507. <https://doi.org/10.2207/qjws.13.500>
8. Homma R, Shinohara Y, Kadoi K, Inoue H (2021) Effect of S and Si on the formation of intragranular ferrite and inclusions in ultra-low oxygen weld metal of low carbon steel. *ISIJ Int* 61(1):309–316. <https://doi.org/10.2355/isijinternational.ISIJINT-2020-112>



9. Mills AR, Thewlis G, Whiteman JA (1987) Nature of inclusions in steel weld metals and their influence on formation of acicular ferrite. *Mater Sci Tech* 3(12):1051–1061
10. Koseki T, Ohkita S, Yurioka N (1997) Thermodynamic study of inclusion formation in low alloy steel weld metals. *Sci Tech Weld Join* 2(2):65–69. <https://doi.org/10.1179/stw.1997.2.2.65>
11. Ito Y, Nakanishi M (1976) Study on Charpy impact properties of weld metal with submerged arc welding. *Sumitomo Search* 15:42–61
12. Evan GM (1992) The effect of titanium in SMA C-Mn steel multi-pass deposits. *Weld J* 71(12):447s–454s
13. Evan GM (1993) Effect of titanium in manganese-containing SMA weld deposit. *Weld J* 72(3):123s–133s
14. Evan GM (1995) Microstructure and properties of ferritic steel welds containing Al ad Ti. *Weld J* 74(8):249s–261s
15. Evan GM (1996) Microstructure and properties of ferritic steel welds containing Ti ad B. *Weld J* 75(8):251s–260s
16. Johnson MQ, Evan GM, Edwards GR (1995) The influence of titanium additions and interpass temperature on the microstructures and mechanical properties of high strength SMA weld metals. *ISIJ Int* 35(10):1222–1231. <https://doi.org/10.2355/isijinternational.35.1222>
17. Seo K, Kim K-h, Kim HJ, Ryoo H, Evans GM, Lee C (2020) Microstructural and inclusion characteristics of C-Mn steel welds at a minimal level of titanium. *Met Mater Int* 26(8):1226–1234. <https://doi.org/10.1007/s12540-019-00390-4>
18. Horii Y (1995) Effect of chemical composition on strength and toughness of welds made by large heat input submerged arc welding, Doctoral thesis, Osaka University, Osaka, Japan. <http://hdl.handle.net/11094/39436>. Accessed 03-03-2024
19. Yamada T, Terasaki H, Komizo Y (2007) Microstructural evolution in low carbon steel Ti-B weld metals with several Al levels quarterly. *J Jap Weld Soc* 25(4):514–518. <https://doi.org/10.2207/qjwjs.25.514>
20. Terashima H, Hart PHM (1983) Proc. Int Conf on 'Effect of residual impurity and micro-alloying elements on weldability and weld properties', TWI, London, Paper 27
21. Yamada T, Terasaki H, Komizo Y (2008) Microscopic observation of inclusions contributing to formation of acicular ferrite in steel weld metal. *Sci Tech Weld Join* 13(2):118–125. <https://doi.org/10.1179/174329308X271797>
22. Takada A, Terasaki H, Komizo Y (2013) Effect of aluminum content on acicular ferrite formation in low carbon steel weld metals. *Sci Tech Weld Join* 18(2):91–97. <https://doi.org/10.1179/1362171812Y.0000000086>
23. Fujiyama N, Shigesato G (2021) Effect of Mn and Al on acicular ferrite formation in SAW weld metal. *ISIJ Int* 61(5):1614–1622. <https://doi.org/10.2355/isijinternational.ISIJINT-2020-407>
24. Milani JM, Saeid T (2020) Acicular ferrite nucleation and growth in API5L-X65 steel submerged arc welded joints. *Mat Sci Tech* 36(13):1398–1406. <https://doi.org/10.1080/02670836.2020.1783774>
25. Seo K, Ryoo H, Kim HJ, Yoon JG, Lee C (2022) Nature of nonmetallic inclusions in electrogas weld metal. *Weld World* 66:379–390
26. Takada A, Terasaki H, Komizo Y (2014) Role of inclusions for formation of acicular ferrite in low carbon steel weld deposits. *IIW Doc II-1886–14*, IIW, Italy
27. Byun J-S, Cho YW, Chung SH, Shim J-H, Lee DN (1999) Nucleation of intragranular ferrite at Ti<sub>2</sub>O<sub>3</sub> particle in low carbon steel. *Acta Mater* 47(9):1751–1760
28. Byun J-S, Shim J-H, Cho YW, Lee DN (2003) Non-metallic inclusion and intragranular nucleation of ferrite in Ti-killed steel. *Acta Mater* 51:1593–1606
29. Li Y, Wan XL, Cheng L, Wu KM (2016) Effect of oxides on nucleation of ferrite: first principle modelling and experimental approach. *Mat Sci Tech* 32(1):88–93. <https://doi.org/10.1179/1743284715Y.0000000102>
30. Seo K, Kim Y-M, Kim HJ, Lee C (2015) Characterization of inclusions formed in Ti-containing steel weld metals. *ISIJ Int* 55(8):1730–1738. <https://doi.org/10.2355/isijinternational.ISIJINT-2014-800>
31. Seo K, Kim Y-M, Evans GM (2015) Formation of Mn-depleted zone in Ti-containing weld metals. *Weld World* 59(3):373–380. <https://doi.org/10.1007/s40194-014-0207-y>
32. Kang Y, Han K, Park JH, Lee C (2015) Variation in the chemical driving force for intergranular nucleation in the multi-pass weld metal of Ti-containing high-strength low-alloy steel. *Met Mater Trans A* 46A(8):2015–3581
33. Homma R, Shigesato G, Fujioka M, Kadoi K, Inoue H (2022) Mn depletion behavior at oxide/matrix interface in low oxygen weld metal of low carbon steel. *Tetsu-to-Hagane* 108(3):211–223. <https://doi.org/10.2355/tetsutohagane.TETSU-2021-087>
34. Wang B, Liu X, WANG G, (2018) Inclusion characteristics and acicular ferrite nucleation in Ti-containing weld metals of X80 pipeline steel. *Met Mater Trans A* 49A(6):2124–2138. <https://doi.org/10.1007/s11661-018-4570-y>
35. Homma R, Kadoi K, Inoue H (2021) Effects of Ti and Al on the formation of intragranular ferrites in the ultra-low-oxygen Si-Mn weld metals of low-carbon steel. *Mater Today Commun* 29:102963. <https://doi.org/10.1016/j.mtcomm.2021.102963>
36. Nakayama K, Kisaya Y, Kimura F, Terasaki H (2020) A study on mechanism of acicular ferrite formation in GMA weld metals. *Quarterly J Jap Weld Soc* 38(4):229–233. <https://doi.org/10.2207/qjwjs.38.229>
37. Rule Requirements for Materials and Welding\_Part 2 (2019), American Bureau Shipping, USA
38. ASTM E23–23a, Standard test methods for notched bar impact testing of metallic materials, ASTM Int, PA, USA, <https://doi.org/10.1520/E0023-23A>
39. Hunt AC, Klucken AO, Edward GR (1994) Heat input and dilution effects in micro-alloyed steel weld metal. *Weld J* 73(1):9s–15s
40. Hidaka T, Suenaga K, Okazaki Y, Ishida H (2009) Influence of oxides on microstructure and notch toughness of weld metal with flux-cored wires for high strength steel quarterly. *J Jap Weld Soc* 27(2):154s–157s. <https://doi.org/10.2207/qjwjs.27.154s>
41. Jia X, Li H, Yang Y, Hao Y, Wang B, Wang B (2024) Evolution of complex oxide inclusions during the smelting process of oxide metallurgical steel and their effect on acicular ferrite nucleation. *Met Mater Trans A* 55A(3):724–753. <https://doi.org/10.1007/s11661-023-0726608>
42. Yamamoto K, Hasegawa T, Katamura J (1996) Effect of boron on intra-granular ferrite formation in Ti-oxide bearing steels. *ISIJ Int* 36(1):80–86. <https://doi.org/10.2355/isijinternational.36.80>
43. Seo JS, Seo K, Kim HJ, Lee C (2014) Effect of titanium content on weld microstructure and mechanical properties of bainitic GMA welds. *Weld World* 58:893–901
44. Pargeter RJ, Dolby RE (1980) A scheme for the quantitative description of ferritic weld microstructures, IIW Doc. IXJ-29–80, IIW, Italy
45. Davey TG, Widgey DJ (1976) A technique for the characterization of weld metal microstructure, IIW Doc. II-389–76, IIW, Italy
46. Farrar RA, Zhang Z (1995) Aspect ratios and morphology of acicular ferrite in C-Mn-Ni weld metals. *Mater Sci Tech* 11(8):759–764

**Publisher's Note** Springer Nature remains neutral with regard to jurisdictional claims in published maps and institutional affiliations.

Springer Nature or its licensor (e.g. a society or other partner) holds exclusive rights to this article under a publishing agreement with the author(s) or other rightsholder(s); author self-archiving of the accepted manuscript version of this article is solely governed by the terms of such publishing agreement and applicable law.